

Anti-dark and Mexican-hat solitons in the Sasa-Satsuma equation on the continuous wave background

Tao Xu¹, Min Li² and Lu Li³

1. *College of Science, China University of Petroleum, Beijing 102249, China,*

E-mail: xutao@cup.edu.cn.

2. *Department of Mathematics and Physics, North China Electric*

Power University, Beijing 102206, China.

3. *Institute of Theoretical Physics, Shanxi University, Taiyuan, Shanxi 030006, China.*

Abstract

In this letter, via the Darboux transformation method we construct new analytic soliton solutions for the Sasa-Satsuma equation which describes the femtosecond pulses propagation in a monomode fiber. We reveal that two different types of femtosecond solitons, i.e., the anti-dark (AD) and Mexican-hat (MH) solitons, can form on a continuous wave (CW) background, and numerically study their stability under small initial perturbations. Different from the common bright and dark solitons, the AD and MH solitons can exhibit both the resonant and elastic interactions, as well as various partially/completely inelastic interactions which are composed of such two fundamental interactions. In addition, we find that the energy exchange between some interacting soliton and the CW background may lead to one AD soliton changing into an MH one, or one MH soliton into an AD one.

PACS numbers: 05.45.Yv; 42.65.Tg; 42.81.Dp

Introduction. — As localized wave packets formed by the balance between the group-velocity dispersion and self-phase modulation [1], solitons in optical fibers have drawn considerable attention because of their robust nature and potential application in all-optical, long-distance communications [2]. In the picosecond regime, the model governing the propagation of optical solitons in a

single-mode fibre is the celebrated nonlinear Schrödinger equation (NLSE) [1]. However, one has to take into account some higher-order linear and nonlinear effects for the ultrashort pulses propagating in high-bit-rate transmission systems [2]. The governing model for the femtosecond pulse propagation is the following higher-order NLSE [3]:

$$i u_z + \frac{\sigma}{2} u_{tt} + |u|^2 u = -i\varepsilon [\sigma_1 u_{ttt} + \sigma_2 (|u|^2 u)_t + \sigma_3 u (|u|^2)_t], \quad (1)$$

where $\sigma = \pm 1$, ε is a real small parameter, σ_1 , σ_2 and σ_3 represent the third-order dispersion (TOD), self-steepening (SS, also known as Kerr dispersion) and stimulated Raman scattering (SRS) effects, respectively [2, 3].

With $\sigma_1 \neq 0$, Eq. (1) has two important integrable versions: (i) the Hirota equation (HE) [4], $\sigma_1 : \sigma_2 : \sigma_2 + \sigma_3 = 1 : 6\sigma : 0$; (ii) the Sasa-Satsuma equation (SSE) [5], $\sigma_1 : \sigma_2 : \sigma_2 + \sigma_3 = 1 : 6\sigma : 3\sigma$. The SSE usually takes the form [5]

$$i u_z + \frac{\sigma}{2} u_{tt} + |u|^2 u + i\varepsilon [u_{ttt} + 6\sigma (|u|^2 u)_t - 3\sigma u (|u|^2)_t] = 0. \quad (2)$$

Although there is a fixed relation among the higher-order terms, the SSE is thought to be more fundamental than the HE for applications in optical fibers because the former contains the SRS term [2, 3]. Up to now, many integrable properties of Eq. (2) have been detailed, like the inverse scattering transform scheme [5, 6], bilinear representation [7], Painlevé property [8], conservation laws [9], nonlocal symmetries [10], squared eigenfunctions [11], Bäcklund transformation [12] and Darboux transformation (DT) [13, 14].

The presence of the SRS term enriches the solitonic behavior in Eq. (2) [5–7, 14–18]. Under the vanishing boundary condition (VBC), Eq. (2) with $\sigma = 1$ possesses the common single-hump soliton [5, 15], the double-hump soliton behaving like two in-phase solitons with a fixed separation [5, 6], and the multi-hump breather with the periodically-oscillating structure [6, 7]. Under the non-vanishing boundary condition, Eq. (2) with $\sigma = -1$ admits the common dark soliton, and the double-hole dark soliton displaying two symmetric dips with a fixed separation [16, 17]; while Eq. (2) with $\sigma = 1$ has the bright-like soliton which is linearly combined of a dark one and a bright one [18]. On the other hand, the soliton interaction behavior underlying in the SSE is far more abundant and complicated than that in the NLSE. Even with the VBC, the shape-changing interactions between soliton and breather have recently been found in Eq. (2) with $\sigma = 1$ [14].

In this letter, we are trying to reveal some novel solitonic phenomena on a continuous wave (CW) background for Eq. (2) with $\sigma = 1$. Via the DT technique [14], we obtain three families of single-soliton solutions which can display two completely-different profiles. The first type is the anti-dark (AD) soliton having the form of a bright soliton on a CW background, i.e., it looks like a dark soliton with reverse sign amplitude [19]. The second type takes the Mexican-hat (MH) shape, that is, one high hump carries two small dips which have a symmetrical distribution with respect to the hump, hence such new type of soliton is called the MH soliton. More importantly, we find that the femtosecond AD and MH solitons admit the resonant interaction, elastic interaction, as well as various partially/completely inelastic interactions which consist of the fundamental resonant and elastic interaction structures. To our knowledge, it is the first time that the coexistence of elastic and resonant soliton interactions has been found in the NLSE-type models. Physically, the resonant interaction of optical waves excited from a CW background can be used to realize a second-harmonic generation in the centro-symmetry optical fiber [20].

N-th iterated soliton solutions via the Darboux transformation. — With the simple CW solution $u = \rho e^{i(\frac{t}{6\varepsilon} - \frac{z}{108\varepsilon^2} + \phi)}$ ($\rho > 0$ and ϕ are both real constants) as a seed, we employ the DT-iterated algorithm presented in Ref. [14] to obtain the N-th iterated solution in the form

$$u_N = e^{i(\frac{t}{6\varepsilon} - \frac{z}{108\varepsilon^2})} \left(\rho e^{i\phi} - 2 \frac{\tau_{N+1, N-1, N}}{\tau_{N, N, N}} \right), \quad (3)$$

with

$$\tau_{J, K, L} = \begin{vmatrix} \mathbf{F}_{N \times J} & -\mathbf{G}_{N \times K} & -\mathbf{H}_{N \times L} \\ \mathbf{F}_{N \times J}^* & -\mathbf{H}_{N \times K}^* & -\mathbf{G}_{N \times L}^* \\ \mathbf{G}_{N \times J}^* & \mathbf{F}_{N \times K}^* & \mathbf{0} \\ \mathbf{H}_{N \times J} & \mathbf{F}_{N \times K} & \mathbf{0} \\ \mathbf{H}_{N \times J}^* & \mathbf{0} & \mathbf{F}_{N \times L}^* \\ \mathbf{G}_{N \times J} & \mathbf{0} & \mathbf{F}_{N \times L} \end{vmatrix}, \quad (4)$$

where $J+K+L = 6N$, the block matrices $\mathbf{F}_{N \times J} = (\lambda_k^{m-1} f_k)_{\substack{1 \leq k \leq N, \\ 1 \leq m \leq J}}$, $\mathbf{G}_{N \times K} = [(-\lambda_k)^{m-1} g_k]_{\substack{1 \leq k \leq N, \\ 1 \leq m \leq K}}$,

$\mathbf{H}_{N \times L} = [(-\lambda_k)^{m-1} h_k]_{\substack{1 \leq k \leq N, \\ 1 \leq m \leq L}}$, and the functions f_k, g_k, h_k ($1 \leq k \leq N$) are given as

$$\begin{cases} f_k = e^{\frac{i\phi}{2}} \left(\alpha_k e^{\theta_k(t,z)} + \beta_k e^{-\theta_k(t,z)} \right), \\ g_k = -e^{-\frac{i\phi}{2}} \left(\frac{\rho \alpha_k}{\chi_k^+} e^{\theta_k(t,z)} + \frac{\rho \beta_k}{\chi_k^-} e^{-\theta_k(t,z)} - \gamma_k e^{-\omega_k(t,z)} \right), \\ h_k = -e^{\frac{3i\phi}{2}} \left(\frac{\rho \alpha_k}{\chi_k^+} e^{\theta_k(t,z)} + \frac{\rho \beta_k}{\chi_k^-} e^{-\theta_k(t,z)} + \gamma_k e^{-\omega_k(t,z)} \right), \end{cases} \quad (5)$$

with $\theta_k(t, z) = \chi_k \left[t - \frac{z}{12\varepsilon} - 4(\lambda_k^2 + \rho^2) \varepsilon z \right]$, $\omega_k(t, z) = \lambda_k \left(t - \frac{z}{12\varepsilon} - 4\lambda_k^2 \varepsilon z \right)$, $\chi_k = \sqrt{\lambda_k^2 - 2\rho^2}$, $\chi_k^\pm = \lambda_k \pm \sqrt{\lambda_k^2 - 2\rho^2}$, α_k, β_k and γ_k being nonzero complex constants.

In order to obtain the solitonic structure from solution (3), we require all χ_k 's ($1 \leq k \leq N$) be real numbers, that is, $\text{Im}(\lambda_k) = 0$ and $|\lambda_k| > \sqrt{2}\rho$. For convenience of our analysis, we introduce the notations $\mu_k^{(1)} = \alpha_k^* \beta_k - \alpha_k \beta_k^*$, $\mu_k^{(2)} = \alpha_k^* \gamma_k + \alpha_k \gamma_k^*$ and $\mu_k^{(3)} = \beta_k^* \gamma_k + \beta_k \gamma_k^*$ ($k = 1, 2$), and use “ (n, m) ” to represent the soliton interaction with n asymptotic solitons as $z \rightarrow -\infty$ and m ones as $z \rightarrow \infty$.

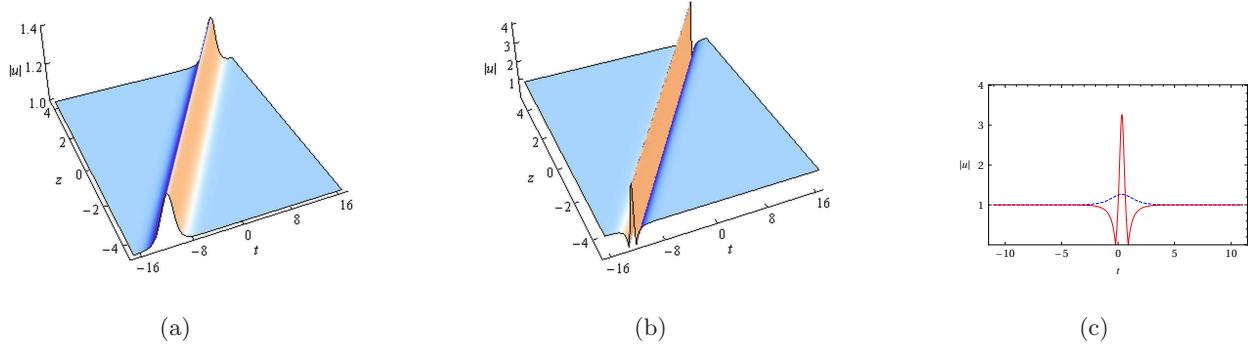


Figure 1: Evolution of the (a) AD soliton and (b) MH soliton plotted via solution (6), where $|\alpha_1| = |\beta_1| = 1$, $\lambda_1 = 1.6$, $\rho = 1$, $\phi = 0$, $\varepsilon = 0.15$, $\phi_1^{(1)} = 0$ for (a) and $\phi_1^{(1)} = \pi$ for (b). (c) Transverse plots of AD (blue dotted line) and MH (red solid line) solitons at $z = 0$.

Anti-dark and Mexican-hat solitons. — For solution (3) with $N = 1$, we can obtain three families of single-soliton solutions under the reducible cases $\mu_1^{(i)} = 0$ ($1 \leq i \leq 3$). If $\mu_1^{(1)} = 0$ (i.e., $\beta_1 \alpha_1^* - \alpha_1 \beta_1^* = 0$), the solution can be written as

$$u_1^{(1)} = \rho e^{i\left(\frac{t}{6\varepsilon} - \frac{z}{108\varepsilon^2} + \phi + \pi\right)} + \frac{\sqrt{2} \chi_1^2 e^{i\left(\frac{t}{6\varepsilon} - \frac{z}{108\varepsilon^2} + \phi + \pi\right)}}{\sqrt{2} \rho + |\lambda_1| e^{i\phi_1^{(1)}} \cosh(\Theta_1^{(1)} + \delta_1^{(1)})}, \quad (6)$$

where $\Theta_1^{(1)} = 2\theta_1(t, z)$, $\delta_1^{(1)} = \frac{1}{2} \ln \left(\frac{|\alpha_1|^2 \chi_1^-}{|\beta_1|^2 \chi_1^+} \right)$, $\phi_1^{(1)} = \text{Arg}(\alpha_1) - \text{Arg}(\beta_1) = 0$ or π . In this solution, the first part $\rho e^{i(\frac{t}{6\varepsilon} - \frac{z}{108\varepsilon^2} + \phi + \pi)}$ is a CW solution of Eq. (2), while the second part describes a soliton embedded in the CW background (Note that the denominator has no singularity because $|\lambda_1| > \sqrt{2}\rho$).

The parameter $\phi_1^{(1)} = 0$ implies that the embedded solution has the same phase as that of the CW solution. In this case, $u_1^{(1)}$ represents an AD soliton which displays the bright soliton profile on the CW pedestal [see Figs. 1(a) and 1(c)]. The soliton velocity and width are, respectively, given by $v = 4\varepsilon(\rho^2 + \lambda_1^2) + \frac{1}{12\varepsilon}$ and $w = \frac{1}{2\lambda_1}$, and $|u_1^{(1)}|$ reaches the maximum $|u_1^{(1)}|_{\max} = \frac{\rho|\lambda_1| + \sqrt{2}(\lambda_1^2 - \rho^2)}{(|\lambda_1| + \sqrt{2}\rho)}$ when $\Theta_1^{(1)} = 0$. If $\phi_1^{(1)} = \pi$, the embedded solution and CW solution have the same phases in the inner region $\frac{\sqrt{2}(\rho^2 + \chi_1^2) - \chi_1 \sqrt{2\lambda_1^2 - \rho^2}}{\rho|\lambda_1|} \leq \Theta_1^{(1)} + \delta_1^{(1)} \leq \frac{\sqrt{2}(\rho^2 + \chi_1^2) + \chi_1 \sqrt{2\lambda_1^2 - \rho^2}}{\rho|\lambda_1|}$, but their phases are opposite in the outer region $\Theta_1^{(1)} + \delta_1^{(1)} < \frac{\sqrt{2}(\rho^2 + \chi_1^2) - \chi_1 \sqrt{2\lambda_1^2 - \rho^2}}{\rho|\lambda_1|}$ or $\Theta_1^{(1)} + \delta_1^{(1)} > \frac{\sqrt{2}(\rho^2 + \chi_1^2) + \chi_1 \sqrt{2\lambda_1^2 - \rho^2}}{\rho|\lambda_1|}$. Hence, the modulus of $u_1^{(1)}$ exhibits that one high hump is symmetrically accompanied with two small dips beneath the CW background, which looks like the MH shape [see Figs. 1(b) and 1(c)]. The velocity and width of the MH soliton are the same as those of the AD one, but its maximum amplitude drastically increases to $|u_1^{(1)}|_{\max} = \frac{\sqrt{2}(\rho^2 + \chi_1^2) - \rho|\lambda_1|}{|\lambda_1| - \sqrt{2}\rho}$ at the center of the hump, and drops to zero at the centers of two dips. The generation of the MH soliton could be explained as that the phase oppositeness makes some energy be transferred from the CW background to the embedded solution, and further leads to rising of one hump and sinking of two dips.

For the reducible cases $\mu_1^{(2)} = 0$ and $\mu_1^{(3)} = 0$, we can obtain the other two families of single-soliton solutions as follows:

$$u_1^{(2)} = e^{i(\frac{t}{6\varepsilon} - \frac{z}{108\varepsilon^2} + \phi)} \left[\rho \tanh(\Theta_1^{(2)} + \delta_1^{(2)}) + e^{i\phi_1^{(2)}} \sqrt{\lambda_1 \chi_1^+} \text{sech}(\Theta_1^{(2)} + \delta_1^{(2)}) \right], \quad (7)$$

$$u_1^{(3)} = e^{i(\frac{t}{6\varepsilon} - \frac{z}{108\varepsilon^2} + \phi + \pi)} \left[\rho \tanh(\Theta_1^{(3)} + \delta_1^{(3)}) + e^{i\phi_1^{(3)}} \sqrt{\lambda_1 \chi_1^-} \text{sech}(\Theta_1^{(3)} + \delta_1^{(3)}) \right], \quad (8)$$

where $\Theta_1^{(2)} = \theta_1(t, z) + \omega_1(t, z)$, $\Theta_1^{(3)} = \theta_1(t, z) - \omega_1(t, z)$, $\delta_1^{(2)} = \frac{1}{2} \ln \left(\frac{|\alpha_1|^2 \chi_1^2}{|\gamma_1|^2 \lambda_1 \chi_1^+} \right)$, $\delta_1^{(3)} = \frac{1}{2} \ln \left(\frac{|\gamma_1|^2 \lambda_1 \chi_1^-}{|\beta_1|^2 \chi_1^2} \right)$, $\phi_1^{(2)} = \text{Arg}(\alpha_1) - \text{Arg}(\gamma_1) = \pm \frac{\pi}{2}$ and $\phi_1^{(3)} = \text{Arg}(\beta_1) - \text{Arg}(\gamma_1) = \pm \frac{\pi}{2}$. Because $|\lambda_1| > \sqrt{2}\rho$, either $u_1^{(2)}$ or $u_1^{(3)}$ displays only the AD soliton profile, which is similar to the case $\phi_1^{(1)} = 0$ in solution (6). Solutions (7) and (8) are also called the combined solitary wave solutions [18]. The combined dark and bright solitons have a constant phase difference $\frac{\pi}{2}$ or $-\frac{\pi}{2}$. Such phase difference causes a

nonlinear phase shift, for example, the nonlinear phase shift in solution (7) can be given as

$$\phi_{\text{NL}}^{(2)}(t, z) = \arctan \left[\sin \phi_1^{(2)} \cdot \frac{\sqrt{\lambda_1 \chi_1^+} \operatorname{sech}(\Theta_1^{(2)} + \delta_1^{(2)})}{\rho \tanh(\Theta_1^{(2)} + \delta_1^{(2)})} \right]. \quad (9)$$

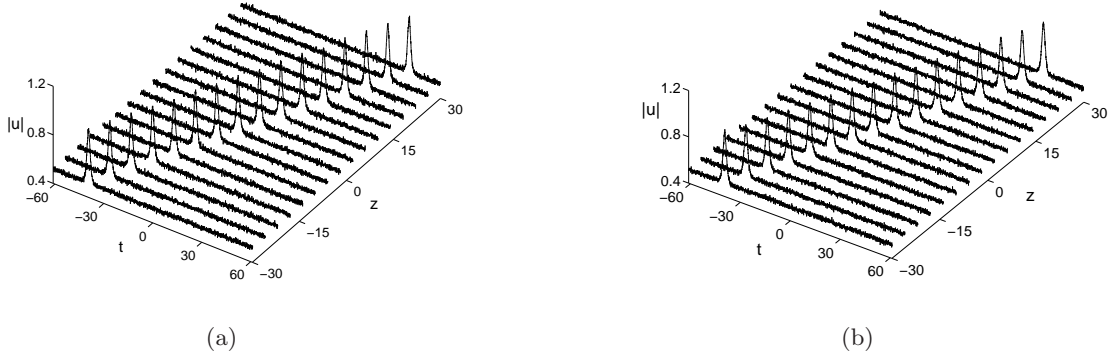


Figure 2: Numerical evolution of the AD soliton under the perturbation of a white noise with the maximal value 0.08. The initial pulse corresponds to solution (6) at $z = 0$ with the parameters as $\alpha_1 = \beta_1 = \lambda_1 = 1$, $\rho = 0.5$, $\varepsilon = 0.13$, (a) $\sigma_1 : \sigma_2 : \sigma_2 + \sigma_3 = 1 : 6 : 3$, (b) $\sigma_1 : \sigma_2 : \sigma_2 + \sigma_3 = 1 : 5.8 : 2.5$.

The stability of solitons is a crucial issue for their applications in optical communication lines [2]. It has been shown in Ref. [18] that the solitons described by solutions (7) and (8) enjoy a good stability against finite-amplitude initial perturbations. Here, the numerical simulation is performed to examine the stability of solution (6) by the split-step Fourier method [2]. Fig. 2(a) shows that with the presence of a white noise, the AD soliton can propagate stably for 60 dispersion lengths along the fiber. Also, we numerically simulate the evolution of the AD soliton when the TOD, SS and SRS terms do not obey the fixed relation in Eq. (2). Fig. 2(b) illustrates that the AD soliton still keeps its stable shape after propagating 60 dispersion lengths when $\sigma_1 : \sigma_2 : \sigma_2 + \sigma_3 = 1 : 5.8 : 2.5$ and the initial pulse is perturbed by a white noise. However, there is some radiation on the background of the MH soliton during the propagation if a white noise is added in the initial pulse. We note that the practical optics telecommunication system is usually dissipative because of the fiber loss/gain [21]. With the inclusion of a linear loss/gain term into Eq. (2), our numerical experiments show that both the AD and MH solitons together with the CW background decay/grow

exponentially with the evolution of z . Thus, the balance between the energy input and output also plays an important role in maintaining a long-lived optical soliton [22].

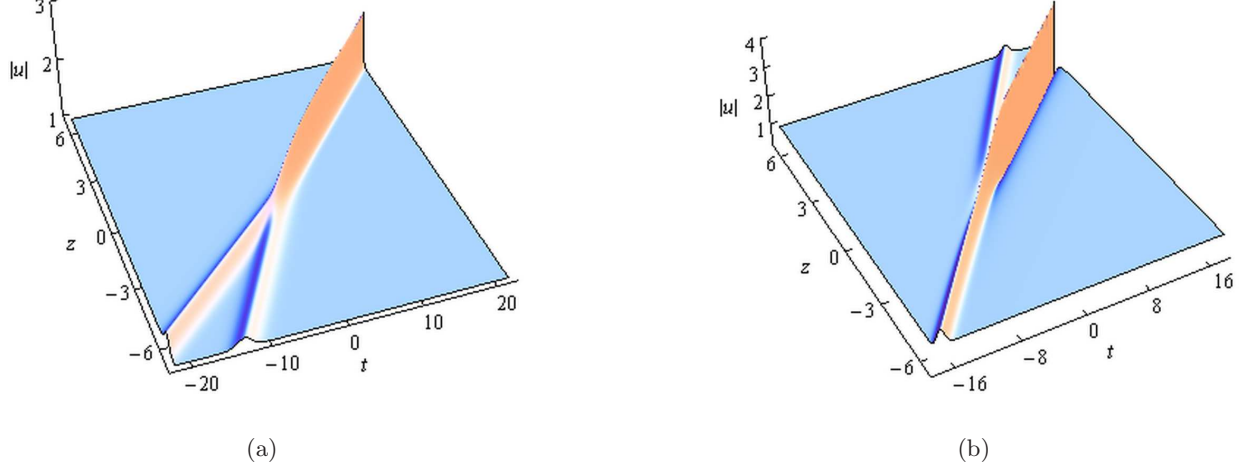


Figure 3: (a) Resonant (2,1)-interaction of three AD solitons with $\lambda_1 = 1.6$ and $\gamma_1 = 1 + 2i$. (b) Resonant (1,2)-interaction of two AD solitons and one MH soliton with $\lambda_1 = -1.42$ and $\gamma_1 = 1 - 2i$. The other parameters are chosen as $\alpha_1 = 1$, $\beta_1 = 1 + i$, $\rho = 1$, $\phi = 0$ and $\varepsilon = 0.25$.

Resonant and elastic interactions. — If $\mu_1^{(i)} \neq 0$ ($1 \leq i \leq 3$) in solution (3) with $N = 1$, the phase difference (which is neither π nor $\pm\frac{\pi}{2}$) between the embedded solution and the CW solution results in that there are three asymptotic solitons appearing on top of the same CW background. The asymptotic expressions of the three solitons as $z \rightarrow \pm\infty$ have the same form in Eqs. (6)–(8) except that

$$\phi_1^{(1)} = \frac{\pi}{2} [1 - \text{sgn}(\mu_1^{(2)} \mu_1^{(3)})], \quad \delta_1^{(1)} = \frac{1}{2} \ln \left(\frac{|\mu_1^{(2)}|^2 \chi_1^-}{|\mu_1^{(3)}|^2 \chi_1^+} \right), \quad (10)$$

$$\phi_1^{(2)} = \frac{\pi}{2} \text{sgn}(i\mu_1^{(1)} \mu_1^{(3)}), \quad \delta_1^{(2)} = \frac{1}{2} \ln \left(\frac{|\mu_1^{(1)}|^2 \chi_1^2}{|\mu_1^{(3)}|^2 \lambda_1 \chi_1^+} \right), \quad (11)$$

$$\phi_1^{(3)} = -\frac{\pi}{2} \text{sgn}(i\mu_1^{(1)} \mu_1^{(2)}), \quad \delta_1^{(3)} = \frac{1}{2} \ln \left(\frac{|\mu_1^{(2)}|^2 \lambda_1 \chi_1^-}{|\mu_1^{(1)}|^2 \chi_1^2} \right). \quad (12)$$

Their wave numbers and frequencies can be respectively given as follows: $(K_1^{(1)}, \Omega_1^{(1)}) = [-8\varepsilon(\rho^2 + \lambda_1^2) \chi_1 - \frac{\chi_1}{6\varepsilon}, 2\chi_1]$, $(K_1^{(2)}, \Omega_1^{(2)}) = [-\frac{\chi_1^+}{12\varepsilon} - 2\varepsilon(\chi_1^+)^2(\lambda_1 + \chi_1^-), \lambda_1 + \chi_1]$, $(K_1^{(3)}, \Omega_1^{(3)}) = [\frac{\chi_1^-}{12\varepsilon} + 2\varepsilon(\chi_1^-)^2(\lambda_1 + \chi_1^+), \chi_1 - \lambda_1]$, which exactly satisfy the three-soliton resonant conditions $K_1^{(1)} = K_1^{(2)} + K_1^{(3)}$ and $\Omega_1^{(1)} = \Omega_1^{(2)} + \Omega_1^{(3)}$. Associated with $\lambda_1 > 0$ and $\lambda_1 < 0$, the solu-

tion can, respectively, exhibit the (2, 1)-resonant structure of two solitons merging into one soliton and the (1, 2)-resonant structure of one soliton diverging into two solitons, as shown in Figs. 3(a) and 3(b). When $\text{sgn}(\mu_1^{(2)} \mu_1^{(3)}) = 1$, the three resonant solitons all belongs to the AD case; while for $\text{sgn}(\mu_1^{(2)} \mu_1^{(3)}) = -1$, two are still the AD solitons but the other one is of the MH shape. That means that the CW background exchanges its energy with one interacting soliton, and causes such soliton changes its shape after resonant interaction, as shown in Fig. 3(b).

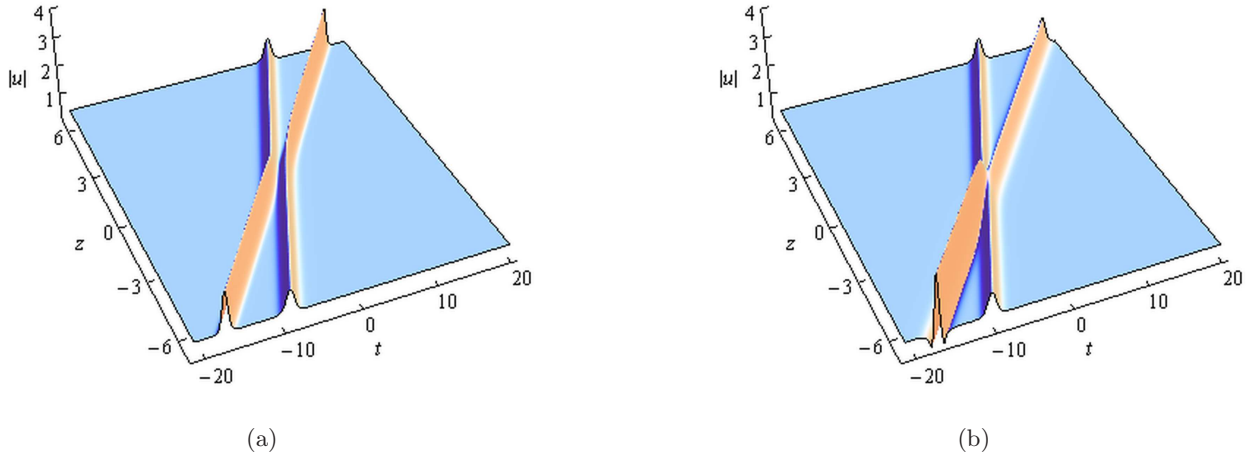


Figure 4: (a) Shape-preserving elastic (2, 2)-soliton interaction with $\alpha_2 = 1 + i$. (b) Shape-changing elastic (2, 2)-soliton interaction with $\alpha_2 = 1$. The other parameters are chosen as $\alpha_1 = 1$, $\beta_1 = i$, $\beta_2 = -1$, $\gamma_1 = 1$, $\gamma_2 = 1 - i$, $\rho = 0.5$, $\lambda_1 = -1$, $\lambda_2 = 1.42$, $\phi = 0$ and $\varepsilon = 0.25$.

On the other hand, one can also obtain the elastic (2, 2)-soliton interactions by implementing the DT two times. Our analysis shows that there are four asymptotic solitons as $z \rightarrow \pm\infty$ in solution (3) with $N = 2$ under the condition $\mu_1^{(i)} = \mu_2^{(j)} = 0$ ($1 \leq i, j \leq 3$). The expressions of asymptotic solitons are still of the form in Eqs. (6)–(8) except that there are some difference for the parameters $\phi_k^{(i)}$ and $\delta_k^{(i)}$ ($k = 1, 2; 1 \leq i \leq 3$) (details are omitted for saving the space). Each interacting soliton could be either the AD or MH one, depending on the concrete parametric choice. For example, Fig. 4(a) illustrates that the AD solitons display the standard elastic interaction, that is, they can completely recover their individual intensities and velocities after an interaction except for the phase shift in their envelopes. Note that the phase shift, which corresponds to the instantaneous frequency at pulse peak being nonzero, will result in the relative motion of interacting solitons [23]. Also, the

energy exchange may take place between some interacting soliton and the CW background, and result in the shape change of such soliton after interaction, as seen in Fig. 4(b). However, this kind of soliton interactions are still considered to be elastic in the sense that there is no energy exchange between two different solitons.

Partially and completely inelastic interactions. — For other cases in solution (3) with $N = 2$, one can obtain five different types of inelastic soliton interactions. If there is only one $\mu_k^{(i)}$ equal to 0, the solution can exhibit the (3,2)- and (2,3)-soliton interactions which are, respectively, associated with $\lambda_{k-3} > 0$ and $\lambda_{k-3} < 0$ [see Figs. 5(a) and 5(b)]. In both the two cases, the numbers of interacting solitons as $z \rightarrow \pm\infty$ are not equal, but one $z \rightarrow -\infty$ soliton and one $z \rightarrow \infty$ soliton [which are marked by the red arrows in Figs. 5(a) and 5(b)] have the same velocities and intensities and differ only by the phases of their envelopes. Accordingly, the (3,2)- and (2,3)-soliton interactions belong to the *partially inelastic type*. If none of $\mu_k^{(i)}$'s ($1 \leq i \leq 3$, $1 \leq k \leq 2$) is equal to 0, the solution can display the (3,3)-, (4,2)- and (2,4)-soliton interactions which are, respectively, associated with $\lambda_1\lambda_2 < 0$, $\lambda_1, \lambda_2 > 0$ and $\lambda_1, \lambda_2 < 0$ [see Figs. 6(a)–6(c)]. Such three interactions are of the *completely inelastic type* in the sense that the asymptotic solitons as $z \rightarrow -\infty$ totally differ from those as $z \rightarrow \infty$ in the velocities and intensities.

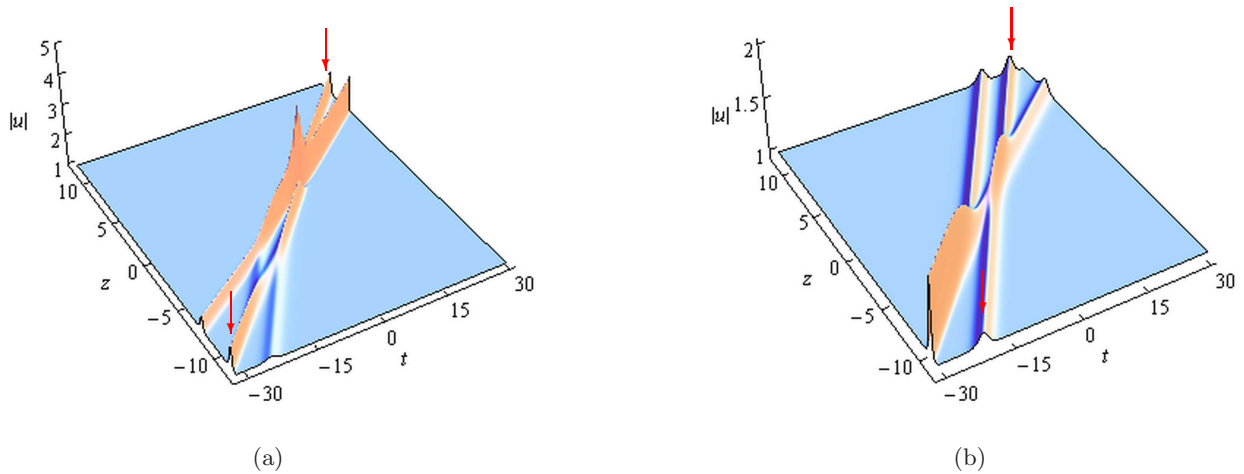


Figure 5: (a) Inelastic (3,2)-soliton interaction with $\beta_1 = 1 + i$, $\beta_2 = 2 + i$, $\gamma_1 = 0.2$, $\lambda_1 = 1.5$ and $\lambda_2 = -1.73$. (b) Inelastic (2,3)-soliton interaction with $\beta_1 = i$, $\beta_2 = 1 + i$, $\gamma_1 = 1$, $\lambda_1 = 1.73$ and $\lambda_2 = -1.5$. The other parameters are chosen as $\alpha_1 = \alpha_2 = \gamma_2 = \rho = 1$, $\phi = 0$ and $\varepsilon = 0.25$.

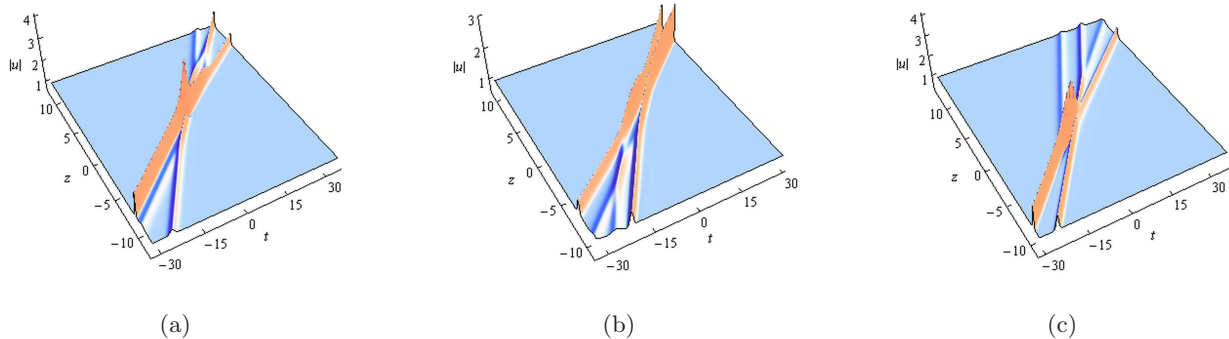


Figure 6: (a) Inelastic (3,3)-soliton interaction with $\alpha_2 = 4$, $\beta_1 = -16i$, $\beta_2 = 1 - 5i$, $\gamma_1 = 2 - i$, $\gamma_2 = 0.5$, $\lambda_1 = 1.5$ and $\lambda_2 = -1.73$. (b) Inelastic (4,2)-soliton interaction with $\alpha_2 = 1 - i$, $\beta_1 = 5i$, $\beta_2 = 10i$, $\gamma_1 = 1 + 10i$, $\gamma_2 = -i$, $\lambda_1 = 1.5$ and $\lambda_2 = 1.73$. (c) Inelastic (2,4)-soliton interaction with $\alpha_2 = 1 - 0.1i$, $\beta_1 = 1 - 10i$, $\beta_2 = i$, $\gamma_1 = 1$, $\gamma_2 = i$, $\lambda_1 = -1.5$ and $\lambda_2 = -1.73$. The other parameters are chosen as $\alpha_1 = 1$, $\rho = 1$, $\phi = 0$ and $\varepsilon = 0.25$.

As for the above five inelastic interactions, we find that in the near-field region the asymptotic solitons connect with one another via the “X”- and “Y”-type junctions, which correspond to the elastic and resonant interactions, respectively. For example, there are three resonant interactions and one elastic interaction in Fig. 5(a), and there appear three resonant interactions in Fig. 5(b). Therefore, the “X”-type elastic interaction and “Y”-type resonant interaction are two fundamental structures to form various complicated soliton interactions in Eq. (2), where the numbers, velocities and intensities of interacting solitons as $z \rightarrow \pm\infty$ are in general not the same.

Conclusion. — In this letter, via the DT method we have constructed new analytic soliton solutions for Eq. (2) which governs the propagation of femtosecond pulses in a monomode fiber with the TOD, SS and SRS effects. We have revealed that two new types of femtosecond solitons (i.e., the AD and MH solitons) occur in Eq. (2) with $\sigma = 1$ on a CW background. The numerical experiments have indicated that the AD soliton can propagate stably for a long distance with presence of a small initial perturbation or slight violation of the fixed ratio of parameters in Eq. (2). More importantly, we have obtained that the AD and MH solitons can exhibit both the resonant and elastic interactions. Such two fundamental interactions can generate various complicated structures, in which the numbers, velocities and intensities of interacting solitons are

usually not the same before and after interaction. In addition, we have found that some interacting soliton may exchange its energy with the background in the interaction, which results in one AD soliton changing into an MH one, or one MH soliton into an AD one. It should be noted that changing the propagation direction of optical solitons is an important concept for realizing optical switching [24]. Therefore, as a self-induced Y-junction waveguide, the soliton resonant interaction might bring about some applications in all-optical information processing and routing of optical signals [2, 24]. In mathematics, our results will enrich the knowledge of soliton interactions in a (1+1)-dimensional integrable equation with the single field. It is also worthy of being studied to make a finer classification of soliton interactions in Eq. (2) with $\sigma = 1$.

Acknowledgements. — This work has been supported by the Science Foundations of China University of Petroleum, Beijing (Grant No. BJ-2011-04), by the National Natural Science Foundations of China under Grant Nos. 11247267, 11371371, 11426105, 61475198, and by the Fundamental Research Funds of the Central Universities (Project No. 2014QN30).

References

- [1] A. Hasegawa and F. Tappert, *Appl. Phys. Lett.* **23**, 142 (1973); **23**, 171 (1973).
- [2] G. P. Agrawal, *Nonlinear Fiber Optics* (5th edition, Academic, Oxford, 2012).
- [3] Y. Kodama, *J. Stat. Phys.* **39**, 597 (1985); Y. Kodama and A. Hasegawa, *IEEE J. Quantum Electron.* **23**, 510 (1987).
- [4] R. Hirota, *J. Math. Phys.* **14**, 805 (1973).
- [5] N. Sasa and J. Satsuma, *J. Phys. Soc. Jpn.* **60**, 409 (1991).
- [6] D. Mihalache, L. Torner, F. Moldoveanu, N.-C. Panoiu, and N. Truta, *Phys. Rev. E* **48**, 4699 (1993).
- [7] C. Gilson, J. Hietarinta, J. Nimmo, and Y. Ohta, *Phys. Rev. E* **68**, 016614 (2003).
- [8] D. Mihalache, N. Truta, and L. C. Crasovan, *Phys. Rev. E* **56**, 1064 (1997).
- [9] J. Kim, Q. Han Park, and H. J. Shin, *Phys. Rev. E* **58**, 6746 (1998).

- [10] A. Sergyeyev and D. Demskoi, J. Math. Phys. **48**, 042702 (2007).
- [11] J. K. Yang and D. J. Kaup, J. Math. Phys. **50**, 023504 (2009).
- [12] O. C. Wright III, Chaos Solitons Fractals **33**, 374 (2007).
- [13] Y. S. Li and W. T. Han, Chin. Ann. Math. Ser. B **22**, 171 (2001).
- [14] T. Xu and X. M. Xu, Phys. Rev. E **87**, 032913 (2013); T. Xu, D. H. Wang, M. Li, and H. Liang, Phys. Scr. **89**, 075207 (2014).
- [15] K. Porsezian and K. Nakkeeran, Phys. Rev. Lett. **76**, 3955 (1996); M. Gedalin, T. C. Scott, and Y. B. Band, Phys. Rev. Lett. **78**, 448 (1997).
- [16] Y. Jiang and B. Tian, EPL **102**, 10010 (2013).
- [17] Y. Ohta, AIP Conference Proceedings **1212**, 114 (2010).
- [18] Z. H. Li, L. Li, H. P. Tian, and G. S. Zhou, Phys. Rev. Lett. **84**, 4096 (2000).
- [19] Yu. S. Kivshar, Phys. Rev. A **43**, 1677 (1991); Yu. S. Kivshar, V. V. Afansjev, and A. W. Snyder, Opt. Commun. **126**, 348 (1996).
- [20] W. N. Cui, G. X. Huang, and B. Hu, Phys. Rev. E **70**, 057602 (2004); W. N. Cui and G. X. Huang, Chin. Phys. Lett. **21**, 2437 (2004).
- [21] X. Liu, D. Han, Z. Sun, et al, Sci. Rep. **3**, 2718 (2013); Y. Cui and X. Liu, Opt. Express **21**, 18969 (2013).
- [22] X. Liu, Phys. Rev. A **81**, 023811 (2010); P. Grelu and N. Akhmediev, Nat. Photon. **6**, 84 (2012).
- [23] X. Liu, Phys. Rev. A **84**, 053828 (2011).
- [24] Yu. S. Kivshar and G. P. Agrawal, *Optical Solitons: From Fibers to Photonic Crystals* (Academic, San Diego, 2003).